Experimental Study of Structure and Dynamics in a Monolayer of Paramagnetic Colloids Confined by Parallel Hard Walls

Ramin Haghgooie,† Chen Li,‡ and Patrick S. Doyle*,†

Department of Chemical Engineering and Department of Physics, Massachusetts Institute of Technology, 77 Massachusetts Avenue, Cambridge, Massachusetts 02139

Received January 11, 2006. In Final Form: February 7, 2006

We study the structural and dynamical properties of paramagnetic colloidal spheres interacting as repulsive dipoles in two dimensions and confined between parallel hard walls. We observed that the structure and dynamics of the self-assembled colloids are strongly dependent upon the width of the confining channel. The system exhibits re-entrant behavior as a function of the channel width, transitioning from solid-like to liquid-like repeatedly in excellent agreement with simulation results. For large channels, an ordered layered structure self-assembles near the walls, but this local structure is not commensurate with the bulk structure, leading to localized stable defects.

1. Introduction

Boundaries can drastically affect the structure of self-assembled colloidal systems either by providing a template for extreme ordering or by disrupting the natural structure of the system.[1−4] In colloidal systems, boundaries can appear in different forms, as an impurity or as a confinement. Self-assembly in the presence of boundaries is of great, and growing, importance in a variety of applications ranging from photonic band gaps and semiconductors[5,6] to medical devices.[7−9] Much research has been done to characterize the effects of boundaries, as well as confinement, upon the self-assembly of colloidal systems because they are both important industrially and from a fundamental scientific standpoint. Much effort has also gone into exerting control over the self-assembly of colloidal systems using boundaries and confinement.[10−12] In particular, 2D colloidal systems are ideal for studying the specifics of self-assembly because of their reduced geometry and their accessible length and time scales.[13,14] Many groups have focused on how boundaries can affect the structure and dynamics of 2D circular clusters of colloids.[15−19] The structure of these systems has been characterized as having an outer region of ringlike structure and an inner region of hexagonal structure, independent of the nature of the circular confining potential.[15−17] This illustrates a case where the boundary imposes an unusual local structure whereas the center of the cluster relaxes back to the unconfined structure.

Recently, the channel-like geometry, or parallel straight walls, has gained importance in this area of research.[20−26] These systems exhibit a layered structure parallel to the confining walls as well as anisotropic diffusion of the colloids, enhanced in the direction parallel to the walls.[20,22,23] Additionally, the nature of the confining potential (hard walls vs softer confinements) can have a strong impact on the types of structures that form in the 2D channel system.[22,24]

Here we present a study of a 2D system of repulsive magnetic dipoles whose self-assembled structure and dynamics exhibit some seemingly contradictory responses to confinement in a 2D channel. Although the confinement induces an organized layered structure near the walls, it also disrupts the hexagonal structure of the system in the same region. Additionally, we observed oscillating behavior in the global structure and dynamics of the system as a function of the width of the confining channel. We show that all of these observations are in excellent agreement with purely predictive simulation results.

2. Experimental Setup

Using soft-lithography,[27] we fabricated poly(dimethylsiloxane) (PDMS) channels 40 μm tall and 40, 80, and 200 μm wide. These channels were treated with an oxygen plasma and bonded to a thin sheet of PDMS such that the two ends of the channel remained open. The channel was filled with a solution of paramagnetic colloidal spheres (2.8 μm carboxylated DynaBeads M-270, Dynal) suspended

* To whom correspondence should be addressed. E-mail: pdoyle@mit.edu. Tel: 617-253-4534. Fax: 617-258-5042.

† Department of Chemical Engineering.

‡ Department of Physics.

(1) Lin, K. H.; Crocker, J. C.; Prasad, V.; Schofield, A.; Weitz, D. A.; Lubensky, T. C.; Yodh, A. G. *Phys. Rev. Lett.* **2000**, *85*, 1770.

(2) Dullens, R. P. A.; Kegel, W. K. *Phys. Rev. Lett.* **2004**, *92*, 195702.

(3) de Villeneuve, V. W. A.; Dullens, R. P. A.; Aarts, D. G. A. L.; Groeneveld, E.; Scherff, J. H.; Kegel, W. K.; Lekkerkerker, H. N. W. *Science* **2005**, *309*, 1231.

(4) Auer, S.; Frenkel, D. *Phys. Rev. Lett.* **2003**, *91*, 015703.

(5) Blanco, A.; Chomski, E.; Grabtchak, S.; Ibisate, M.; John, S.; Leonard, S. W.; Lopez, C.; Meseguer, F.; Miguez, H.; Mondia, J. P.; Ozin, G. A.; Toader, O.; van Driel, H. M. *Nature* **2000**, *405*, 437.

(6) Saado, Y.; Golosovsky, M.; Davidov, D.; Frenkel, A. *Phys. Rev. B* **2002**, *66*, 195108.

(7) Stendahl, J. C.; Li, L.; Claussen, R. C.; Stupp, S. I. *Biomaterials* **2004**, *25*, 5847.

(8) Zhao, B.; Hu, H.; Mandal, S. K.; Haddon, R. C. *Chem. Mater.* **2005**, *17*, 3235.

(9) Doyle, P. S.; Bibette, J.; Bancaud, A.; Viovy, J.-L. *Science* **2002**, *295*, 2237.

(10) van Blaaderen, A.; Ruel, R.; Wiltzius, P. *Nature* **1997**, *385*, 321.

(11) Guo, Q.; Arnoux, C.; Palmer, R. E. *Langmuir* **2001**, *17*, 7150.

(12) Su, G.; Guo, Q.; Palmer, R. E. *Langmuir* **2003**, *19*, 9669.

(13) Löwen, H. *Phys. Rev. E* **1996**, *53*, R29.

(14) Zahn, K.; Lenke, R.; Maret, G. *Phys. Rev. Lett.* **1999**, *82*, 2721−2724.

(15) Lai, Y.-J.; I, L. *Phys. Rev. E* **2001**, *64*, 015601(R).

(16) Kong, M.; Partoens, B.; Peeters, F. M. *Phys. Rev. E* **2003**, *67*, 021608.

(17) Kong, M.; Partoens, B.; Matulis, A.; Peeters, F. M. *Phys. Rev. E* **2004**, *69*, 036412.

(18) Schweigert, I. V.; Schweigert, V. A.; Peeters, F. M. *Phys. Rev. Lett.* **2000**, *84*, 4381.

(19) Bubeck, R.; Bechinger, C.; Neser, S.; Leiderer, P. *Phys. Rev. Lett.* **1999**, *82*, 3364.

(20) Teng, L.-W.; Tu, P.-S.; I, L. *Phys. Rev. Lett.* **2003**, *90*, 245004.

(21) Segalman, R. A.; Hexemer, A.; Kramer, E. J. *Phys. Rev. Lett.* **2003**, *91*, 196101.

(22) Piacente, G.; Schweigert, I. V.; Betouras, J. J.; Peeters, F. M. *Phys. Rev. B* **2004**, *69*, 045324.

(23) Haghgooie, R.; Doyle, P. S. *Phys. Rev. E* **2004**, *70*, 061408.

(24) Haghgooie, R.; Doyle, P. S. *Phys. Rev. E* **2005**, *72*, 011405.

(25) Kumacheva, E.; Carstecki, P.; Wu, H.; Whitesides, G. M. *Phys. Rev. Lett.* **2003**, *91*, 128301.

(26) Helseth, L. E.; Backus, T.; Johansen, T. H.; Fischer, T. M. *Langmuir* **2005**, *21*, 7518.

(27) Xia, Y.; Whitesides, G. M. *Angew. Chem., Int. Ed.* **1998**, *37*, 550.

10.1021/la0601051 CCC: $33.50
Published on Web 03/18/2006

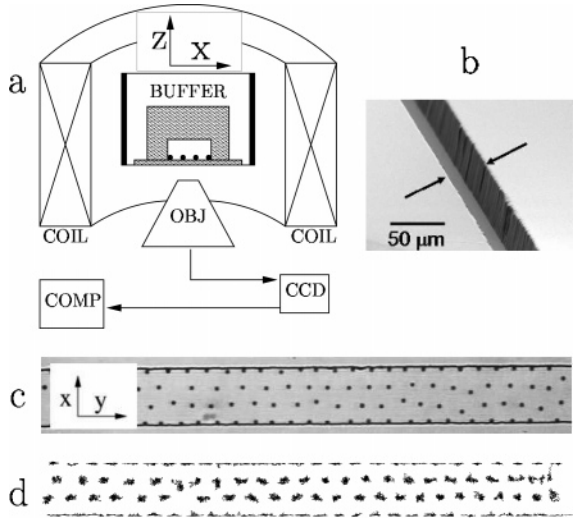

Figure 1. (a) Schematic of the experimental setup (not to scale). An end view of the channel is shown with the shaded regions being PDMS. The beads sediment in the *z* direction to the bottom of the channel. The entire channel system is submerged in TBE buffer inside a chamber and placed into the center of the magnetic coil. The system is observed from underneath with the microscope objective (20×), and the images are captured with a CCD camera and sent to the computer for analysis. (b) SEM image of the PDMS channel before it is sealed. The opening shown will be the bottom of the well once the channel is sealed with a thin sheet of PDMS. The arrows indicate the location of the walls of the channel. (c) Characteristic image obtained during an experiment. The channel width is 40 μm, and the dimensionless channel width is 3.44. (d) Trace of the positions of the colloids in part c for a dimensionless time of 0.65.

in 5.0× TBE buffer (0.17 M ionic strength) to screen the electrostatic repulsion between the colloids. At this ionic strength, the Debye length is ∼1 nm. The colloids have a magnetic susceptibility of 1 (given by the manufacturer)[28] and a specific gravity of 1.6, causing them to sediment in the *z* direction to the bottom of the channel because of gravity, forming a monolayer in the $x-y$ plane with out-of-plane thermal fluctuations of less than ∼80 nm. The open ends of the microchannel were then sealed using Vaseline, and the entire channel system was submerged in TBE buffer inside a sealed chamber with dimensions of ∼2 cm × 2 cm × 2 cm in order to prevent evaporation and pressure-driven flows within the channel. The cell was placed inside an electromagnetic coil (25 mm i.d.) such that the channel was located in the center of the coil, thus causing the system to experience a uniform magnetic field in the *z* direction (normal to the monolayer of colloids). The magnetic field was calibrated using an axial Hall probe and Gauss meter (SYPRIS) and was found to be uniform within a circle of radius 1 cm in the center of the coil. The uniform field induced parallel dipole moments in the colloids causing them to experience purely repulsive interactions.[29] The magnetic coil was placed on an inverted microscope (Axiovert 40 CFL, Zeiss), and image stacks of the system were captured using a CCD camera (KPM1A, Hitachi). A schematic of the experimental setup is shown in Figure 1a, and an SEM image of one of the PDMS channels (before bonding) is shown in Figure 1b. An example of an experimental image is shown in Figure 1c. The image stacks were analyzed off-line using custom programs[30] written in the IDL language (Research Systems, Boulder, CO), allowing us to assemble trajectories for the colloids such as the one shown in Figure 1d.

The characteristic length scale in this system is determined by the number density of colloids (n) and is defined as $R = (\sqrt{3}/2n)^{0.5}$.[14,24] The number density of colloids is defined as the number of colloids divided by the area of the 2D channel accessible to the centers of the colloids. R is the only relevant length scale in this system as long as $d \ll R$, where d is the colloid diameter. Using this length scale, the dimensionless field (Γ) is defined as

$$\Gamma = \frac{\mu_0 M^2}{4\pi k_B T R^3} \tag{1}$$

where μ_0 is the magnetic permeability of free space, k_B is the Boltzmann constant, T is the system temperature, and M is the dipole moment of an individual colloid and is a function of the external magnetic field strength.[23,29] All of the parameters in eq 1 are in SI units. The dipole moment of an individual colloid is defined as

$$M = \frac{4}{3}\pi\left(\frac{d}{2}\right)^3 \frac{\chi}{\mu_0} B \tag{2}$$

where χ is the effective magnetic susceptibility of a single colloid and is ∼1. The energy of interaction between colloids i and j is thus defined as

$$V_{ij} = \Gamma k_B T \left(\frac{R}{r_{ij}}\right)^3 \tag{3}$$

where r_{ij} denotes the scalar distance between the centers of colloids i and j. The dimensionless channel width $\tilde{w}$ was defined as the real channel width divided by R. Using the current in the magnetic coil and the number density of colloids in the system as free parameters, we were able to explore a large section of the $\Gamma - \tilde{w}$ phase space. We varied the dimensionless width of the channels between experiments by changing n, keeping $d \ll R$ for all of the channel widths. We performed experiments for a dimensionless field strength of $\Gamma \approx 12 \pm 1$ (in the liquid phase in the unbounded system[14,31,24]). The precise value of Γ could be measured only after an accurate value for n was obtained during the off-line analysis of the experiment; therefore, during an experiment, we aimed for $\Gamma \approx 12$.

After filling the channel with magnetic colloids, allowing them to sediment, and estimating n for a given system, the magnetic field was turned on, and the system was equilibrated for several tens of dimensionless times. We measured the surface diffusion coefficient of the colloids to be ∼52% of the calculated Stokes diffusion coefficient (D_0). Time was made dimensionless with the time required for a colloid to diffuse freely one unit length along the PDMS surface ($\tilde{t} = 0.52 D_0 t/R^2$). After equilibration, 1000 images were taken over a dimensionless time of ∼15 and were used to analyze the structural and dynamical properties of the system. By repeating several experiments at fixed conditions and obtaining identical results each time, we ensured that the size of the system and the time over which statistics were taken were sufficiently large to represent the equilibrium state of the system. The calculated properties were then compared with results from Brownian dynamics (BD) simulations performed as previously described.[23,24] These simulations do not have any fitted parameters because all of the physical properties in the experiments were known a priori (or measured) for the beads, coil, and channels.

3. Structural Oscillations

The most characteristic global property of the structure in this system is the layering of the colloids parallel to the channel walls.[20,23] This layering is illustrated in the density profiles shown in Figure 2 from the experimental system (dotted lines) and from BD simulations (gray solid lines). For all of the channel widths, there is very good agreement between the simulation results and the experimental results. Slight differences arise at the walls of the channel where the experimental peak heights show some variance with respect to each other and the simulation results.

(28) Dynal reports the magnetic susceptibility of a single M-270 bead to be 60×10^{-5} m^3/kg. When nondimensionalized with the bead density for use in SI units, the result $\chi = 0.96$ is obtained.

(29) Zahn, K.; Méndez-Alcaraz, J. M.; Maret, G. *Phys. Rev. Lett.* **1997**, *79*, 175−178.

(30) Crocker, J. C.; Grier, D. G. *J. Colloid Interface Sci.* **1996**, *179*, 298.

(31) Kalia, R.; Vashishta, P. *J. Phys. C* **1981**, *14*, L643.

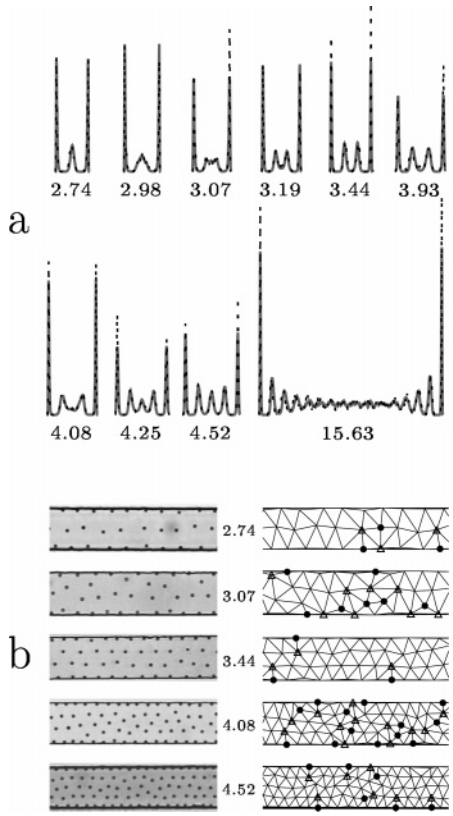

Figure 2. (a) Density profiles across the channels for 10 different dimensionless channel widths 2.74, 2.98, 3.07, 3.19, 3.44, 3.93, 4.08, 4.25, 4.52, and 15.63. The solid gray curve corresponds to the predictions from BD simulations, and the dotted black curves correspond to the density profile measured experimentally. (b) Snapshots of the experimental system and Delaunay triangulations for five different dimensionless channel widths 2.74, 3.07, 3.44, 4.08, and 4.52. All of the channels shown have a true width of 40 μm. Open triangles are seven-coordinated colloids (five-coordinated if next to the wall), and closed circles are five-coordinated colloids (three-coordinated if next to the wall).

In the PDMS channels, the walls are not perfectly planar (Figure 1b), and this roughness gives rise to the differences in the peak heights that we observe experimentally. To accurately and quantitatively capture the effects of the rough walls in the density profiles generated from our BD simulations, we obtained an estimate for the standard deviation of the wall position from our experiments and used that information to approximate "rough walls" during the postprocessing of the simulations. A schematic of this process is presented in Figure 3. The experimental distribution of the wall position was determined by tracing the position of each wall colloid for the duration of the 1000 frames and taking the outermost x position (normal to the wall) as the location of the wall in the vicinity of that colloid. We were then able to assemble a distribution of wall positions for the channel. For a typical experiment, the wall position was measured to have a standard deviation of $\sim$0.3 μm. In postprocessing the simulation results, a random Gaussian variable was added to the x position of the wall colloids with the same standard deviation as measured from the experiment. Even with the presence of rough walls, however, both the experiments and the simulations exhibit very large peaks at the walls, indicating the high degree of localization that occurs at the hard wall.

Another important property to note is the periodic broadening and sharpening of the peaks in the center of the channel as the channel width is increased (Figure 2a). This behavior implies that there are structural changes occurring in the center of the channel as a function of the dimensionless channel width. To study these structural changes in more detail, we used the experimental images to perform a Delaunay triangulation on the positions of the colloids to determine the nearest neighbors and the locations of the defect sites in the channel as shown in Figure 2b. A colloid was considered to be a defect if it had more or less than six neighbors. In the case of flat walls, we have to treat the colloids at the walls differently than those in the bulk. We define the wall colloids as any colloid located within a distance of $^{R}/_{2}$ from the wall, and wall colloids are considered to be defects if they have more or less than four neighbors. The results in Figure 2b show clearly that the structure in the narrow channels is oscillating between order and disorder (low and high defect concentrations) as the channel width is increased.

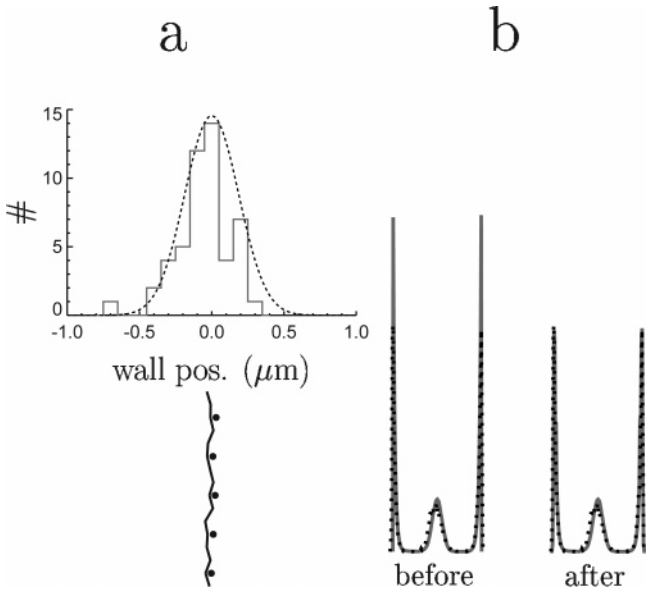

Figure 3. (a) (Top) Distribution of wall positions for a dimensionless channel width of 2.74 is shown as the gray histogram, and the Gaussian curve with the same mean and standard deviation as the histogram is shown as a dashed black line. (Bottom) Schematic of one channel wall illustrating the roughness and how the wall colloids can be used to probe that roughness. (b) Comparison of experimental (dotted black) and simulation (solid gray) density profiles for a dimensionless channel width of 2.74 before and after the simulation data have been corrected for wall roughness.

A similar set of structural transitions has been noted previously for hard-sphere systems confined in thin slits (3D systems).[32,33] However, in the case of hard spheres in thin slits, the structural transitions are the result of geometric constraints upon the packing of the spheres resulting in transitions from one type of solid crystal structure to another. The 3D system can transition from a triangular to square lattice and back as the thin gap height is increased.[32] In the case of repulsive dipoles confined in 2D channels, the system remains in a triangular lattice at all channel widths, but the lattice lines alternate between straight (parallel to the walls) and buckled as the channel width is increased. Additionally, in the 2D channel system, the structural transitions are intimately tied to changing dynamics in the system, which we will discuss shortly.

For the largest channel shown in Figure 2a, the layering near the walls is seen to give way to an isotropic (liquid) structure in the center of the channel for this dimensionless field strength. This feature strongly resembles the structure of a hard-sphere fluid near a flat hard wall. In the case of hard spheres, the wall

(32) Pieranski, P.; Strzelecki, L.; Pansu, B. *Phys. Rev. Lett.* **1983**, *50*, 900.
(33) Neser, S.; Bechinger, C.; Leiderer, P. *Phys. Rev. Lett.* **1997**, *79*, 2348.

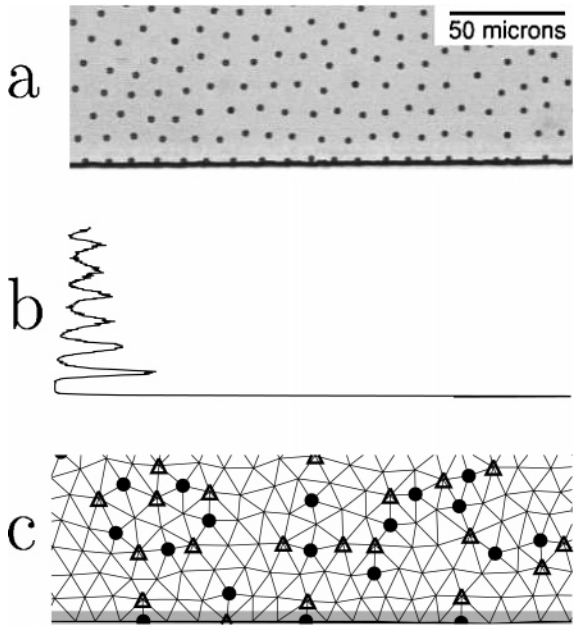

Figure 4. (a) Experimental image for a section of a channel with $\tilde{w} = 15.63$ showing the structure near the wall. (b) Density profile in the section of the channel shown in part a. (c) Delaunay triangulation for the section of the channel shown in part a. The shaded region at the bottom represents the wall region (at a distance less than $R/2$ from the wall). Open triangles are seven-coordinated colloids (five-coordinated if in the wall region), and closed circles are five-coordinated colloids (three-coordinated if in the wall region).

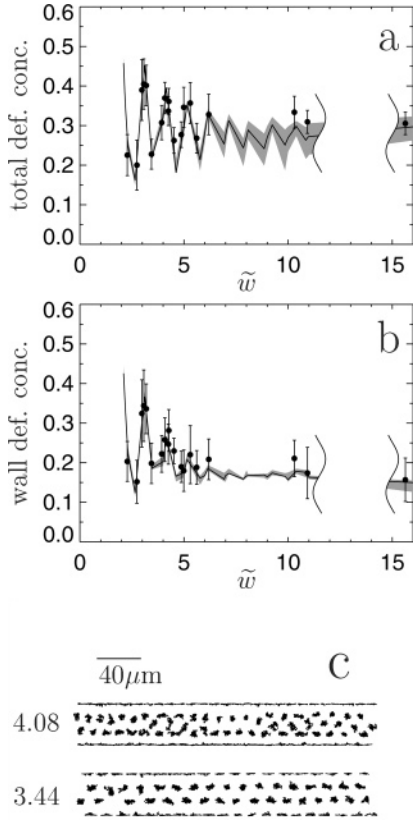

Figure 5. Defect concentration as a function of the dimensionless channel width at a dimensionless field strength of 12 ± 1 for (a) the channel as a whole and (b) the wall region. The solid line represents the simulation results for $\Gamma = 12$ with the shaded region representing the range of defect concentrations for $\Gamma = 12 \pm 1$. The closed circles represent the experimental data. (c) Colloid trajectories in two different channel widths (4.08 and 3.44) at $\Gamma = 12 \pm 1$ for a dimensionless time of 0.65.

can act as a nucleation site for a perfect, layered crystal to form out of the fluid phase.[4] However, in the case of repulsive dipoles in 2D next to a hard wall, this is not exactly what happens. The long-ranged nature of the colloidal interaction combined with the presence of a hard wall leads to a higher concentration of colloids along the wall than in the bulk for large channels.[23] This concentration difference causes the appearance of dislocations along the wall, as seen in Figure 4c, resulting in a seemingly contradictory response of this system to the presence of a flat hard wall. In Figures 2a and 4b, the dimensionless channel width of 15.63 clearly exhibits a more crystalized (layered) state near the walls, but we show that although the wall assists in the natural formation of a crystal it also induces regularly spaced defects in that crystal. Furthermore, as seen in Figure 4c, the first layer in the bulk corrects the structure, and the dislocations along the wall no longer strongly affect the structure of the rest of the system.

The appearance of dislocations along the wall is an interesting phenomenon seen in different forms in other systems. The large channel limit in hard-wall channels is essentially equivalent to a hard circular confinement with infinite radius. Kong et al.[17] showed that large 2D clusters confined in hard-wall circles exhibit a large number of defects along the confining boundary. More recently, de Villeneuve et al.[3] studied a 2D slice of a 3D hard sphere colloidal system near a spherical impurity, using confocal microscopy. The spherical impurity created a convex boundary in the 2D slice. In this case, they observed regular grain boundaries emanating radially outward from the circular boundary similar to the regularly spaced dislocations observed in our 2D hard-wall channel system. However, there are significant differences between these three examples. In the large 2D clusters as well as the convex boundary case, the defects along the confining boundary are attributed to the bending of the lattice whereas in our system the lattice does not need to bend at the boundary. Additionally, in the case of the convex boundary, the defects continue to radiate out into the bulk as grain boundaries whereas in our system they are terminated after the first layer in the bulk.

4. Structure and Dynamics

Having located the defect sites in our system, we were also able to calculate the average concentration of defects for a given set of conditions. The results for the total and wall defect concentrations are shown in Figure 5a and b, respectively. We observed very pronounced oscillating behavior in the total defect concentration (Figure 5a) in our experimental system. We note that for very narrow channels the total defect concentration closely follows that of the wall defect concentration because most of the colloids in the system are wall colloids. However, above a dimensionless channel width of ~5 the wall behavior begins to deviate from that of the total defect concentration. As predicted,[23] in the large channel limit, the wall defect concentration goes to a constant value not equal to zero because of the presence of stable dislocations along the wall.

The defect concentration is intimately tied to the dynamics of the system; therefore, the dynamical behavior of the system also oscillates as a function of the dimensionless channel width. In Figure 5c, the two traces shown are for a peak (4.08) and valley (3.44) in the defect concentration curve shown in Figure 5a. The channel with the higher defect concentration (4.08) exhibits more liquid-like dynamics, with some of the colloids able to diffuse away more easily from their original positions in a short time. For the lower defect concentration (3.44), the colloidal crystal

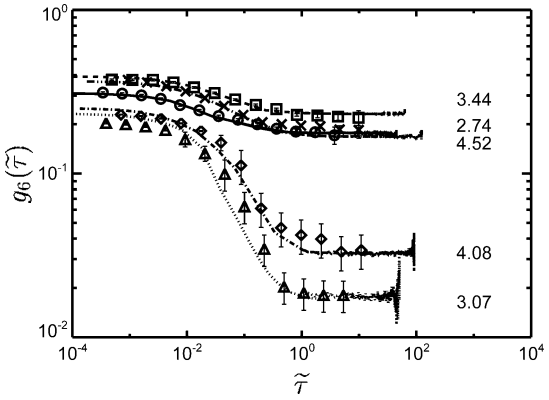

Figure 6. Bond-order correlation function as a function of time for five different dimensionless channel widths 2.74 (−○−), 3.07 (••△••), 3.44 (--□--), 4.08 (-•◇-•), and 4.52 (-•••×-•••). The lines represent results from BD simulations, and the symbols are experimental results.

appears to be more solid-like with the colloids remaining on their original lattice sites.

A more quantitative measure of the dynamics in the system is the bond-order correlation function in time, or $g_6(\tilde{\tau})$.[34] The bond-order correlation function in time can be a measure of the phase of the system with the solid phase having a constant value of g_6 in time whereas g_6 decays exponentially to zero in the liquid phase. The bond-order correlation function in time is given by the expression

$$g_6(\tilde{\tau}) = \langle \Psi_6^*(0)\, \Psi_6(\tilde{\tau}) \rangle \tag{4}$$

where $\tilde{\tau}$ is the dimensionless lag time and Ψ_6 is the local-bond-order parameter

$$\Psi_6 = \frac{1}{m} \sum_{k=1}^{m} e^{i6\theta_k} \tag{5}$$

In eq 5, m is the number of nearest neighbors for a given colloid and θ_k is the angle between the vector connecting the colloid and its kth nearest neighbor and an arbitrary reference axis. The nearest neighbors are determined by performing a Delaunay triangulation. In the 2D channel system, the behavior of $g_6(\tilde{\tau})$ for the colloids in the bulk (at a distance greater than $R/2$ from the wall) can be used as a measure of the state of the system.[24] In Figure 6, we show $g_6(\tilde{\tau})$ data for the five dimensionless channel widths shown in Figure 2b from both simulations and experiments. As the dimensionless channel width is increased from 2.74 to 4.52, the $g_6(\tilde{\tau})$ behavior of the system oscillates between a solid-like constant for $\tilde{w} = 2.74$, 3.44, and 4.52 and a liquid-like decay for $\tilde{w} = 3.07$ and 4.08. All of the curves in Figure 6 show the characteristic intermediate-time plateau in $g_6(\tilde{t})$ that is expected for thin channels, but they illustrate the re-entrant behavior of the system, transitioning from liquid-like to solid-like and back as the channel width is increased.[24] Previous authors have theoretically predicted similar re-entrant behavior for another

(34) Nelson, D. *Phase Transitions and Critical Phenomena*; Domb, C., Lebowitz, J. L., Eds.; Academic Press: London, 1983.

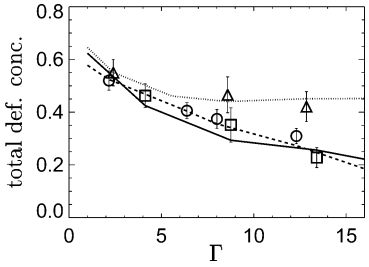

Figure 7. Total defect concentration as a function of Γ for three different dimensionless channel widths 3.07 (△), 3.41 (□), and 10.93 (○). The lines represent simulation results for $\tilde{w} = 3.07$ (•••), 3.41 (−), and 10.93 (---).

2D system (in parabolic confinement),[22] but this is the first experimental observation of re-entrant behavior as a function of confining geometry for 2D repulsive colloidal systems.

Contrary to these results are the observations for colloids confined in 2D circles[18,19] where re-entrant behavior is reported as a function of the dimensionless field strength. In Figure 7, we show that there is no such re-entrant behavior as a function of dimensionless field strength in this system. However, we do note that the behavior of the system as a function of the dimensionless field strength is strongly dependent upon the dimensionless width of the channel. For $\tilde{w} = 3.07$, increasing Γ does not greatly affect the concentration of defects in the system whereas for $\tilde{w} = 3.41$ the concentration of defects decreases significantly as Γ is increased. For wider channels such as $\tilde{w} = 10.93$, increasing Γ causes a decrease in the total defect concentration because, as mentioned previously, the large channels have a bulk region that behaves more like the unbounded system (without walls).

In summary, we have studied the structure of self-assembled repulsive paramagnetic colloids confined in 2D hard-wall channels. We have observed a global layered structure in the channels as well as evidence of oscillations in the defect concentrations and re-entrant behavior in the dynamics in these systems. In addition, the specifics of the self-assembly next to the hard wall have also been discussed, and we have shown that although the wall does induce an ordered layered structure in this system it also causes defects to form along the wall, disrupting the natural lattice. All of the data are in excellent agreement with purely predictive BD simulations and illustrate the importance of boundaries as well as confinement in determining the structure of self-assembled colloids in 2D systems. We have shown an example where confining boundaries are used to both promote stability and disrupt natural structure in a single colloidal system.

Acknowledgment. We gratefully acknowledge the support of NSF NIRT grant no. CTS-0304128 for this project.

Supporting Information Available: Detailed information for experiments including characteristic length scales R, external magnetic field strength B, and dimensionless field strength Γ for each dimensionless channel width. This material is available free of charge via the Internet at http://pubs.acs.org.

LA0601051